3528–3536 *Nucleic Acids Research, 2017, Vol. 45, No. 6* *Published online 28 November 2016*
doi: 10.1093/nar/gkw1171

siRNA carrying an (*E*)-vinylphosphonate moiety at the 5′ end of the guide strand augments gene silencing by enhanced binding to human Argonaute-2

Elad Elkayam[1,2,3], Rubina Parmar[4], Christopher R. Brown[4], Jennifer L. Willoughby[4], Christopher S. Theile[4], Muthiah Manoharan[4,*] and Leemor Joshua-Tor[1,2,3,*]

[1]Keck Structural Biology Lab, Cold Spring Harbor, NY 11724, USA, [2]Howard Hughes Medical Institute, Cold Spring Harbor, NY 11724, USA, [3]Cold Spring Harbor Laboratory, Cold Spring Harbor, NY 11724, USA and [4]Alnylam Pharmaceuticals, 300 Third Street, Cambridge, MA 02142, USA

Received September 02, 2016; Revised November 03, 2016; Editorial Decision November 08, 2016; Accepted November 09, 2016

ABSTRACT

Efficient gene silencing by RNA interference (RNAi) *in vivo* requires the recognition and binding of the 5′- phosphate of the guide strand of an siRNA by the Argonaute protein. However, for exogenous siRNAs it is limited by the rapid removal of the 5′- phosphate of the guide strand by metabolic enzymes. Here, we have determined the crystal structure of human Argonaute-2 in complex with the metabolically stable 5′-(*E*)-vinylphosphonate (5′-*E*-VP) guide RNA at 2.5-Å resolution. The structure demonstrates how the 5′ binding site in the Mid domain of human Argonaute-2 is able to adjust the key residues in the 5′-nucleotide binding pocket to compensate for the change introduced by the modified nucleotide. This observation also explains improved binding affinity of the 5′-*E*-VP -modified siRNA to human Argonaute-2 *in-vitro*, as well as the enhanced silencing in the context of the trivalent *N*-acetylgalactosamine (GalNAc)-conjugated siRNA in mice relative to the un-modified siRNA.

INTRODUCTION

The minimal complex required to achieve silencing through small interfering RNA (siRNA) in human cells is composed of human Argonaute-2 (hAgo2) and a short guide RNA (20–23 bp) (1). Following formation of this RNA-induced silencing complex (RISC), target mRNA recognition is an extremely rapid process that results in target mRNA cleavage by hAgo2 and ultimately leads to mRNA degradation (2). Though there are numerous points of contact between the protein and the guide RNA backbone, the 5′-phosphate binding site, which is located primarily in the Mid domain with some contributions from the PIWI domain of hAgo2, stands out as the most exquisite and critical. A combination of ionic and hydrogen-bonding interactions ensures accurate positioning of the 5′-phosphate of the guide strand and results in precise cleavage at a single position on the mRNA target (1,3–5). The utilization of siRNAs for therapeutic purposes has revolutionized the field of drug discovery, and a number of siRNA-based compounds have advanced into clinical studies (6,7). This has brought the field closer to the realization of RNAi-based therapies for a number of previously 'undruggable' targets (6,7). Several compounds that are currently undergoing clinical testing are based on a strategy that results in safe and effective siRNA delivery to the liver. The strategy utilizes a synthetic trivalent *N*-acetylgalactosamine (GalNAc) ligand conjugated to the 3′ terminus of the sense strand of the siRNA. The GalNAc moiety binds to the asialoglycoprotein receptor (ASGPR), which is expressed on the cell surface of hepatocytes (8).

An issue that limits exogenous siRNA activity *in vivo* is the rapid removal of the 5′-phosphate of the siRNA by metabolic enzymes (9–11). The lack of a 5′-phosphate results in inefficient incorporation of the guide strand (also called the antisense strand), into hAgo2 (10). Chemical modification of the 5′-phosphate, such as 5′-(*E*)-vinylphosphonate (5′-*E*-VP), mimics phosphate properties while maintaining metabolic stability that could lead to more efficient guide incorporation into hAgo2 and therefore silencing (9,10,12–15). Although 5′-*E*-VP is a known nucleoside modification utilized as a substrate for phosphate binding enzymes since 1976 (16), the evaluation of this modification as a phosphate mimic in siRNAs has been reported only recently (9,10,12–15). Additional internucleotide metabolic stability of siRNAs is attained by replacing the 2′-hydroxyl with the methoxy group (2′-OMe) or fluoro group (2′-F) in addition to phosphorothioate (PS) linkages between the nucleotides (8,17–22).

*To whom correspondence should be addressed. Tel: +1 516 367 8821; Fax: +1 516 367 8873; Email: leemor@cshl.edu
Correspondence may also be addressed to Muthiah Manoharan. Email: mmanoharan@alnylam.com

Here, we solved the crystal structure of hAgo2 in complex with a guide RNA carrying a 5′-*E*-VP modification and studied the effect of the modification on binding to the enzyme. hAgo2 can perfectly accommodate the modified RNA by slightly altering the 5′-phosphate binding site, which also increases the affinity of the 5′-*E*-VP-modified RNA to hAgo2 compared with that of an siRNA with a canonical 5′-phosphate. In addition, 5′-*E*-VP-modified siRNA had higher potency both *in vitro* and *in vivo* than an siRNA of the same sequence with the same backbone linkages and sugar modifications but with a 5′-phosphate.

MATERIALS AND METHODS

Oligonucleotide synthesis and analysis

Oligonucleotides were synthesized on an ABI Synthesizer using commercially available RNA amidites, 5′-*O*-(4,4′-dimethoxytrityl)-2′-deoxy-2′-fluoro-, and 5′-*O*-(4,4′-dimethoxytrityl)-2′-*O*-methyl- 3′-*O*-(2-cyanoethyl-*N*,*N*-diisopropyl) phosphoramidite monomers of uridine, 4-*N*-acetylcytidine, 6-*N*-benzoyladenosine and 2-*N*-isobutyrylguanosine using standard solid-phase oligonucleotide synthesis and deprotection protocols. 5′-VPu containing oligonucleotides were synthesized and deprotected following a modified protocol described in (9,10). The GalNAc ligand was covalently linked to the 3′-end of the sense (S) strand of the siRNA by a phosphodiester linkage between the pyrrolidine scaffold as described (8,10). Phosphorothioate linkages were introduced by oxidation of phosphite utilizing 0.1 M 3-((*N*,*N*-dimethylaminomethylidene)amino)-3H-1, 2, 4-dithiazole-5-thione (DDTT) in pyridine. After deprotection, ion-exchange HPLC purification followed by annealing of equimolar amounts of complementary strands provided the desired siRNA duplex by heating to 90°C and slow cooling. The siRNA samples were analyzed by mass spectrometry and capillary gel electrophoresis and for endotoxin and osmolality as described (8,10).

hAgo2-5′-(*E*)-vinylphosphonate TTR RNA complex structure determination

RNA-free hAgo2 was expressed and purified as previously described (23). The protein was then mixed with 5′-*E*-vinylphosphonate-2′-*O*-methyl-uridine-modified TTR RNA at a 1:1.5 ratio. The complex was purified on a Superdex 200 10/300 increase column (GE Lifesciences) and crystallized as previously described (23). X-ray diffraction data were collected at beamline 19-ID at the Advanced Photon Source at Argonne National Laboratory. Diffraction data were indexed, integrated, and scaled with autoPROC (24). The structure was solved by molecular replacement using the protein chain of the hAgo2 structure as a search model (PDB 4F3T) with PHASER (25). The molecular replacement solution was subjected to rigid body refinement in PHENIX (26) followed by simulated annealing refinement prior to iterative manual model building in COOT (27). Final translation/libration/screw motion (TLS) refinement of the model was performed with PHENIX with manually selected TLS groups (Version 1.10.1-2155). The final structure was refined to R_{work} and R_{free} values of 0.195 and 0.242, respectively. Figures were generated with PyMOL (the PyMOL Molecular Graphics System Version 1.6, Schrödinger).

hAgo2 filter binding assays

^{32}P-labeled TTR RNA (100 pM) was incubated with 2-fold serial dilutions (125 nM to 3.8 pM) of RNA-free hAgo2 for 30 min. Samples were applied to a slot blot apparatus as described in (28). The protein–RNA complex was captured on a nitrocellulose membrane, and the free RNA was captured on a subsequent nylon membrane. For the competition assays, increasing concentrations of the competing RNA and 100 pM of the labeled RNA were mixed with 1 nM (final concentration) of RNA-free hAgo2 and incubated for 30 min. The protein-bound and unbound radiolabeled RNA were visualized by phosphorimaging (Typhoon 7000, GE Healthcare) and quantified using GeneTools software (Synoptics). The results of three experiments were analyzed using Prism software (GraphPad). Data are shown as means of bound RNA/(bound RNA+unbound RNA) plus and minus the standard deviation (SD). For the competition assays results are shown as mean of [1 – (bound RNA/(bound+unbound RNA))] ± SD.

In vitro gene silencing experiments

For transfection into primary mouse hepatocytes, 7.4 μl of Opti-MEM and 0.1 μl of Lipofectamine RNAiMax (Invitrogen) were added to 2.5 μl of siRNA per well of a 384-well plate and incubated at room temperature for 15 min. To each well was added 40 μl of William's E Medium (Life Technologies) containing ∼5×10^3 primary mouse hepatocytes. Cells were incubated for 24 h prior to RNA isolation. The RNA quantification was done using standard PCR methods as previously described (8,29). Values are plotted as a fraction of untreated control cells. Each sample was run in technical duplicate, and each point represents the mean of two biological samples ± % error. *GAPDH* served as the internal control. IC_{50} values were determined and dose response curves were generated using XLFit software.

In vivo gene silencing experiments

All procedures using mice were conducted by certified laboratory personnel using protocols consistent with local, state, and federal regulations. Experimental protocols were approved by the Institutional Animal Care and Use Committee, the Association for Assessment and Accreditation of Laboratory Animal Care International (accreditation number: 001345), and the Office of Laboratory Animal Welfare (accreditation number: #A4517-01). C57BL/6 female mice, aged 6–8 weeks, acquired from Charles River Laboratories were dosed subcutaneously with a volume of 10 μl/g of body weight ($n = 3$ per group). The control group received phosphate buffered saline (PBS). Liver samples were collected from animals dosed with 5′-HO-TTR and 5′-*E*-VPu-TTR siRNA 7 days post-dose. TTR mRNA levels were quantified using the methods described earlier (8).

Quantification of whole liver and Ago2-associated siRNA levels

Mice were sacrificed on day 7 post-dose, and livers were snap frozen in liquid nitrogen and ground into powder for further analysis. Total siRNA liver levels were measured by reconstituting liver powder at 10 mg/ml in PBS containing 0.25% Triton-X 100. The tissue suspension was further ground with 5-mm steel grinding balls at 50 cycles/s for 5 min in a tissue homogenizer (Qiagen TissueLyser LT) at 4°C. Homogenized samples were then heated at 95°C for 5 min, briefly vortexed and allowed to rest on ice for 5 min. Samples were then centrifuged at 21 000 x *g* for 5 min at 4°C. The siRNA-containing supernatants were transferred to new tubes. siRNA sense and guide strand levels were quantified by stem loop reverse transcription followed by Taqman PCR (SL-RT QPCR) based on a previously published method (9,30).

Ago2-bound siRNA from mouse liver was quantified by preparing liver powder lysates at 100 mg/ml in lysis buffer (50 mM Tris–HCl, pH 7.5, 150 mM NaCl, 2mM EDTA, 0.5% Triton-X 100) supplemented with freshly added protease inhibitors (Sigma-Aldrich, P8340) at 1:100 dilution and 1 mM PMSF (Life Technologies). Total liver lysate (10 mg) was used for each Ago2 immunoprecipitation (IP) and control IP. Anti-Ago2 antibody was purchased from Wako Chemicals (Clone No.: 2D4). Control mouse IgG was from Santa Cruz Biotechnology (sc-2025). Protein G Dynabeads (Life Technologies) were used to precipitate antibodies. Ago2-associated siRNAs were eluted by heating (50 μl PBS, 0.25% Triton; 95°C, 5 min) and quantified by SL-RT QPCR as described (10,30).

RESULTS

The 5′ binding pocket of hAgo2 can accommodate modified RNA nucleotides

We previously described a simple and robust method to produce significant amounts of RNA-free hAgo2 (23). This method allows us to load hAgo2 with a particular guide RNA and to measure the binding affinity of any oligonucleotide to hAgo2. Here, we used this method to load hAgo2 with an oligonucleotide modified on the 5′ terminus with 5′-(*E*)-vinylphosphonate 2′-*O*-methyl (2′-OMe)-uridine (5′-*E*-VPu) (Figure 1A). The sequence used in this study was the mouse analogue of an siRNA guide strand designed to target the mRNA encoding transthyretin (TTR), a protein that misfolds and accumulates as amyloid fibrils in patients with certain forms of amyloidosis (31). The sequence of the RNA oligonucleotide modified with 5′-*E*-VPu (5′-*E*-VPu-TTR RNA) is shown in Figure 1C. The complex was crystallized and the structure determined to 2.5-Å resolution (Supplementary Table S1).

The overall structure of the complex is very similar to that of the complex of hAgo2 with unmodified miR-20a (23). 5′-*E*-VPu-TTR RNA is threaded along the Mid, PIWI, N, and PAZ domains with the modified 5′-end anchored in the Mid domain and the 3′-end in the PAZ domain (Figure 1B). Despite sequence differences, the 5′-*E*-VPu-TTR modified guide RNA superimposes almost perfectly with the miR-20a guide RNA of the previously solved miR-20a-hAgo2 complex. The RMSD is 0.347 Å for nucleotides 2–10 and is 1.215 Å overall (Figure 1C and Supplementary Figure S1A). Previous structural studies of Argonaute complexes established that all interactions between eukaryotic Argonautes and the guide RNA beyond that with the first nucleotide are mediated by the phosphate/sugar backbone in a sequence-independent manner (23,28,32–35).

Almost all of the differences between the 5′-*E*-VPu-TTR RNA and the miR-20a RNA are restricted to the 5′ nucleotide (Figure 1D and Supplementary Figure S1B). The position of the phosphorous atom of the 5′ moieties of the two guide RNAs are perfectly aligned between the two structures underlining the precise organization of that binding site. The non-bridging oxygens of the 5′-*E*-VPu moiety are slightly rotated compared to the 5′-phosphate of miR-20a, but the distances between side chains that compose the 5′-phosphate binding site, namely, K533, K570, K566, and R812 side chains and the C-terminal carboxylate of A859 are similar in both structures. The double bond of the 5′-*E*-VPu moiety, which replaces the bridging oxygen of a canonical phosphate, produces a 1-Å shift in the position of the sugar group and the uracil base relative to the positions in miR-20a. Strikingly, all the hAgo2 residues that interact with both the sugar ring and the uracil base are shifted accordingly to accommodate the change in their positions. Y529, an essential residue in the 5′-phosphate binding pocket, is similarly tilted in the complex with 5′-*E*-VPu-TTR RNA, preserving the stacking interaction with the uracil base and maintaining the interaction between its hydroxyl group and one of the oxygens of the 5′-phosphate. In addition, this 1-Å movement brings the uracil base close to the specificity loop, G524-T526, which reads the identity of the first nucleotide base, by 0.7 Å. This results in a much tighter interaction of the Watson-Crick edge and the backbone carbonyl oxygen of G524 than is observed with miR-20a and interactions with the amide groups of G524 and K525 that are not observed in the complex with the unmodified RNA (Figure 1D).

Finally, Q548, which interacts with the 2′-OH of the unmodified nucleotide in the 5′ position of miR-20a, interacts with the oxygen of the 2′-OMe of the 5′-*E*-VPu modification demonstrating that the change from a hydroxyl to a methoxy group did not interfere with binding. Therefore, neither the (*E*)-vinylphosphonate nor the 2′-sugar modification of the 5′-end of the guide strand disrupts binding to hAgo2 and features of this modification may enhance binding in the 5′ binding pocket of hAgo2. Thus, replacing the 5′-P of a guide RNA with the modified 5′-*E*-VPu and the hydroxyl group to a methoxy are not only possible, but appear to be favorable for hAgo2 binding over a 'natural' 5′-nucleotide with a phosphate.

The 5′-(*E*)-vinylphosphonate modification at the 5′-end of the guide strand increases affinity for hAgo2

To test the effect of the 5′-*E*-VPu modification, we measured binding affinities of various TTR guide RNAs of the same sequence and RNA-free hAgo2 using a filter-binding assay (Table 1). A ^{32}P-labeled TTR guide RNA with no chemical modifications had a binding affinity of 1.1 nM for hAgo2 (Figure 2A), which is ∼50 times tighter than

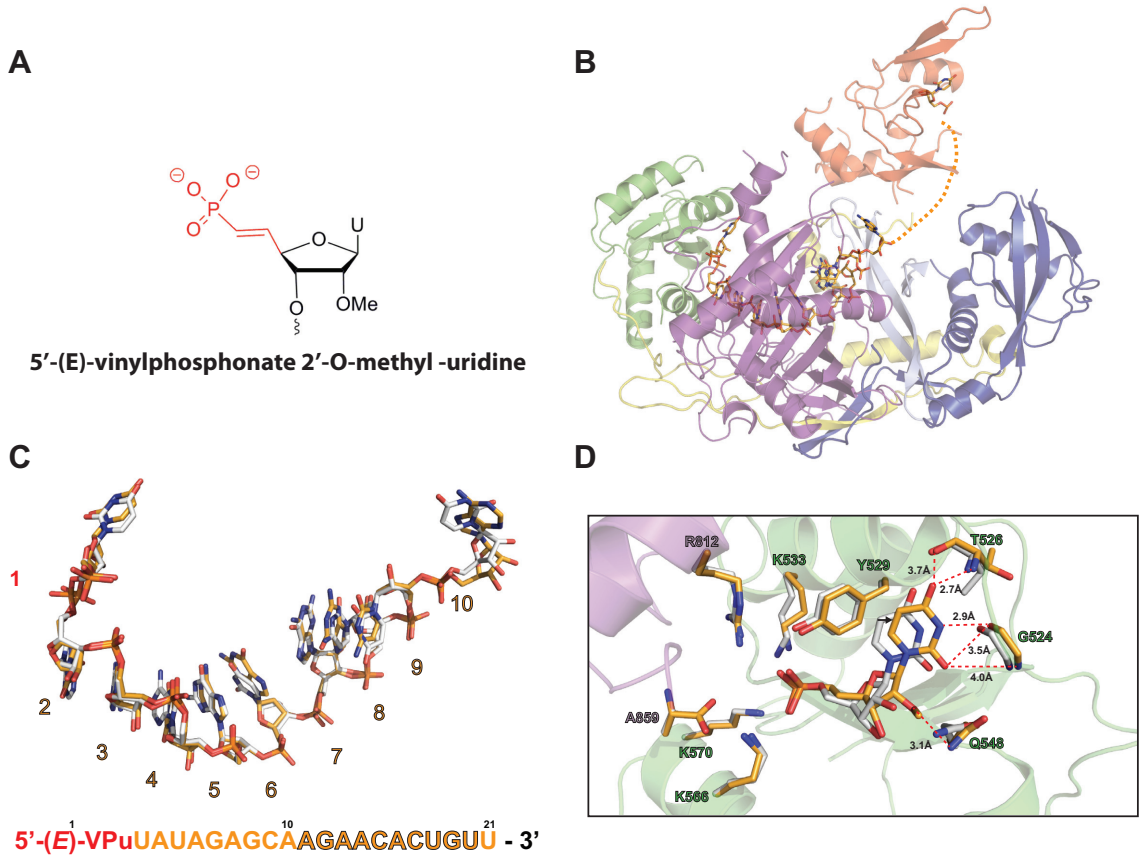

Figure 1. The crystal structure of hAgo2 in complex with 5′-*E*-VPu-TTR guide RNA. (**A**) The chemical structure of 5′-(*E*)-vinylphosphonate 2′-*O*-methyl (2′-OMe)-uridine used in the modified guide RNA. (**B**) Overall structure of hAgo2 in complex with 5′-*E*-VPu-TTR RNA with the N-domain in blue, the L1 domain in light blue, the PAZ domain in red, the L2 domain in yellow, the Mid domain in green, and the PIWI domain in purple. The RNA is colored in gold; the dashed gold line represents bases 11–20, which are disordered in the structure. (**C**) Superposition of phosphate backbones of 5′-*E*-VPu-TTR RNA (gold) and miR-20a from its complex with hAgo2 (23) (PDB 4F3T (white)). The sequence of TTR RNA is shown, red indicates 5′-*E*-VP-modified uridine nucleotide, bases 1–10 and 21 are shown in gold, and disordered bases 11–20 are shown in gold with black outline. (**D**) Comparison of the 5′-phosphate binding pocket in the 5′-*E*-VPu-modified RNA complex (gold) with the miR-20a complex (white).

the previously reported affinity of a GST-hAgo2 expressed in *Escherichia coli* for a single-stranded guide RNA (36). Since the 5′-*E*-VPu-modified oligonucleotide cannot be easily ^{32}P-labeled, we tested binding of the modified RNAs in a competition assay. Here, hAgo2, unmodified ^{32}P-labeled TTR guide RNA, and increasing concentrations of unlabeled 5′-*E*-VPu-TTR guide were mixed together and assayed in a slot blot apparatus. The 5′-*E*-VPu-TTR RNA bound hAgo2 with a dissociation constant of 0.49 nM, ∼2-fold higher affinity than the 5′-P TTR guide (Figure 2B). Similarly, the chemically modified 5′-*E*-VPu-TTR guide oligonucleotide containing sugar modifications and phosphorothiate linkages in addition to the 5′-*E*-VPu modification had a K_d of 0.36 nM, an affinity similar to that of the oligonucleotide with only the 5′-*E*-VPu modification, suggesting that the increased affinity is solely the result of the vinylphosphonate modification (Figure 2C). Moreover, the affinity of a chemically modified RNA with a 5′-OH (K_d = 3.8 nM) was about 10 times lower than that of the 5′-*E*-VPu-TTR guide (Figure 2D). Taken together, these results confirm that the 5′-*E*-VP modification increases the affinity of the guide RNA for hAgo2 resulting from changes in the 5′ binding pocket that are induced by the vinylphosphonate modification.

VP-siRNA-GalNAc conjugates are more potent than their 5′-OH counterparts

Conjugation of a GalNAc ligand to the sense strand of an siRNA results in accumulation in hepatocytes after subcutaneous administration. For analysis of the effect of the 5′-(*E*)-vinylphosphonate modification *in vitro* and *in vivo*, we chose to use the well-characterized GalNAc-conjugated siRNA targeting *TTR* (8). siRNAs were chemically modified at specified positions as shown in Table 2. siRNAs with the 5′-*E*-VPu modification on the guide strand were compared to those harboring a 5′-hydroxyl (5′-OH). siRNA–GalNAc conjugates were transfected into primary mouse hepatocytes and levels of *TTR* were quantified. As shown in Table 2, 5′-*E*-VPu-TTR siRNA was ∼2-fold more potent than 5′-OH-TTR siRNA. These data are consistent with the improved binding of the 5′-*E*-VPu-modified guide RNA.

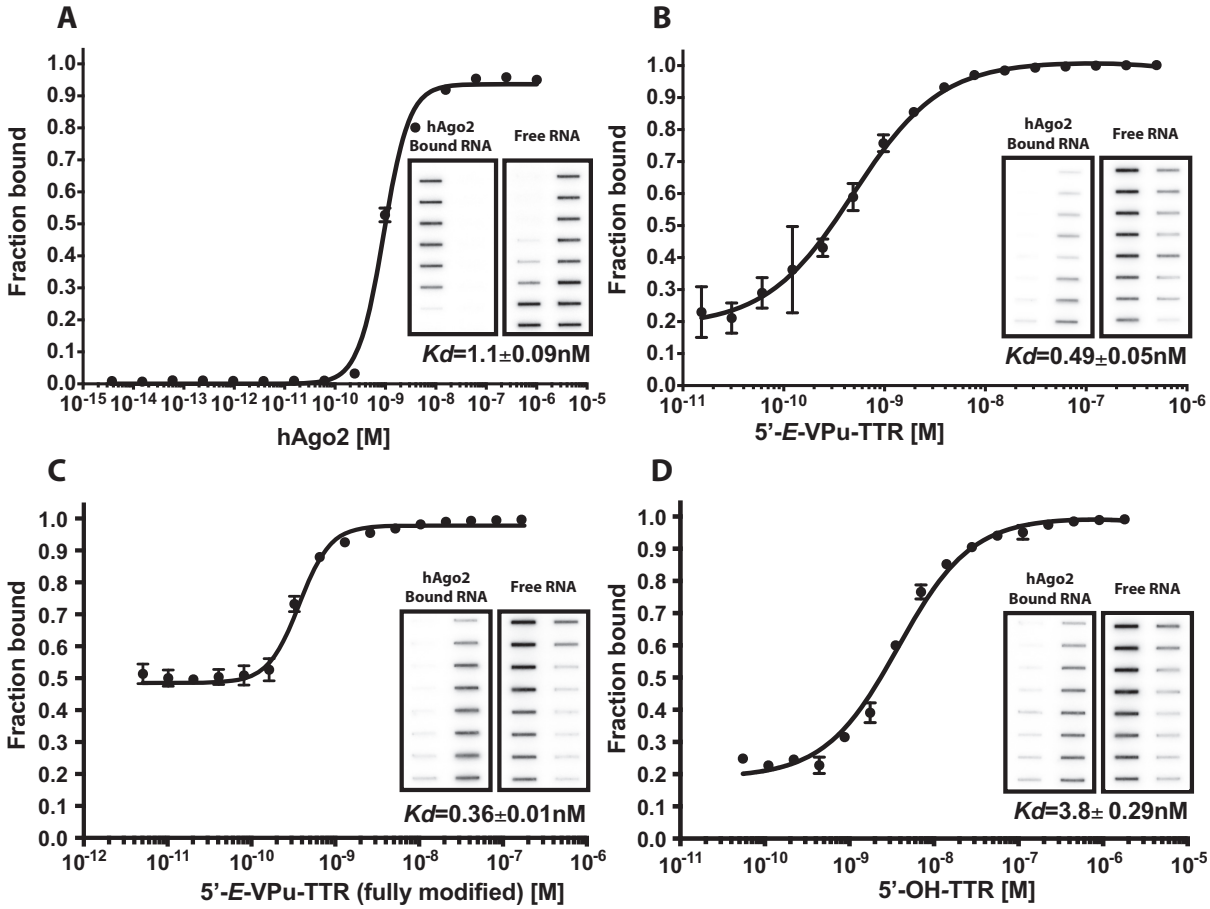

Figure 2. Binding affinity of modified and non-modified guide RNAs to hAgo2. (**A**) *In vitro* binding of radiolabeled 5′-P-TTR RNA to hAgo2. Fraction bound as determined by the filter-binding assay is plotted vs. hAgo2 concentration. (**B**) Competition binding assay of 5′-*E*-VPu-TTR RNA with 5′-P-TTR. Fraction of labeled 5′-P-TTR bound to hAgo2 as a function of 5′-*E*-VPu-TTR concentration is plotted. (**C**) Competition binding assay with chemically modified 5′-*E*-VPu-TTR (see Table 2 for a list of modifications). (**D**) Competition binding assay with chemically modified 5′-OH-TTR. Dissociation constants were calculated from three independent experiments and are presented as means ± standard deviations (SD).

Table 1. Binding affinities of the different guide RNAs to hAgo2

Guide RNA	Dissociation constant (K_d)
TTR (no modifications)	1.1 ± 0.09 nM
5′-*E*-VPu-TTR	0.49 ± 0.05 nM
5′-*E*-VPu-TTR (fully modified)	0.36 ± 0.01 nM
5′-OH-TTR	3.8 ± 0.29 nM

Dissociation constants of the different guide RNAs tested in Figure 2. Dissociation constants from at least three different experiment are shown as means ± standard devations (sd). For the full list of all the modification for 5′-*E*-VPu-TTR (fully modified) see Table 2.

Table 2. Double-stranded oligonucleotides used for *in vitro* and *in vivo* silencing assays

Conjugate ID	Sense strand/guide strand[a]	IC_{50} (nM)[b]
5′-OH-TTR	5′-*A*•a•*C*a*G*u*G*u*UCU*u*Gc*U*c*U*a*U*a*A*GalNAc-3′/ 5′-u•*U*•a*U*a*G*a*G*c*A*aga*A*c*A*c*U*g*U*u•u•u-3′	0.06
5′-*E*-VPu-TTR (fully modified)	5′-*A*•a•*C*a*G*u*G*u*UCU*u*Gc*U*c*U*a*U*a*A*GalNAc-3′/ 5′-VPu•*U*•a*U*a*G*a*G*c*A*aga*A*c*A*c*U*g*U*u•u•u-3′	0.035

[a]Italicized upper case and normal lower case letters indicate 2′-fluoro (2′-F) and 2′-OMe sugar modifications, respectively. The • indicates a phosphorothioate linkage. GalNAc indicates hydroxyprolynyl tri-valent *N*-acetyl-galactosamine linked as previously reported (8). VP indicates the 5′-(*E*)-vinylphosphonate modification.
[b]Half-maximal inhibitory concentration (IC_{50}) of siRNA transfected into primary mouse hepatocytes. siRNA-GalNAc conjugates were tested in primary mouse hepatocytes after lipid transfection. Levels of *TTR* were quantified by RT-PCR and normalized to levels of *GAPDH*.

5′ *E*-VP-siRNA-GalNAc conjugates reduce TTR mRNA levels and incorporate into hAgo2 better than 5′-OH-siRNA-GalNAc conjugates *in vivo*

Next, siRNA-GalNAc conjugates were evaluated for target silencing *in vivo*. Mice were treated with a single subcutaneous dose of 1 mg/kg. At 7 days post-dose, 5′-*E*-VPu-TTR siRNA reduced levels of liver *TTR* mRNA by about 85% relative to levels in control mice, whereas the 5′-HO-TTR siRNA reduced *TTR* levels by ∼64% (Figure 3A). To further investigate the effect of the 5′-*E*-VPu modification, we quantified total liver and Ago2-incorporated levels of the sense and antisense strands as previously described (29,30). Although total siRNA liver levels for the 5′-HO-TTR and 5′-*E*-VPu-TTR GalNAc conjugates were similar (Figure 3B), the amount of 5′-*E*-VPu-TTR guide in complex with Ago2 was about 5-fold higher than the amount of 5′-OH guide (Figure 3C). These data suggest that improvement in potency of the 5′-*E*-VPu-TTR siRNA relative to the siRNA with a guide strand bearing a 5′-OH was due to higher level of incorporation of the 5′-*E*-VPu-TTR guide strand into a complex with Ago2.

DISCUSSION

The use of siRNAs for therapeutic purposes has revolutionized the field of drug discovery, making possible the specific reduction in levels of otherwise 'undruggable' disease-causing proteins. The two main obstacles for the use of siRNA-based therapies is the rapid degradation of exogenous RNAs by several cellular mechanisms on the one hand, and efficient delivery on the other. Several siRNAs that are currently in clinical testing were designed based on a strategy that results in safe and effective siRNA delivery to the liver (6–8). This is achieved by adding a trivalent GalNAc ligand conjugated to the 3′ terminus of the sense (or passenger) strand. In order to overcome their inherent instability, siRNAs are strategically modified with sugar and backbone chemical modifications. Prime among the limitations of exogenous siRNA activity *in vivo* is the rapid removal of the 5′-phosphate of the siRNA. The lack of a 5′-phosphate results in inefficient incorporation of the guide strand (antisense strand) into a complex with Ago2 (10), as well as a decrease in the fidelity of target slicing (1). We have previously shown that the metabolically stable phosphate mimic 5′-*E* vinylphosphonate can be used successfully to overcome this hurdle and showed higher *in vivo* incorporation levels into hAgo2 (10). However, it was still unclear whether improved incorporation is a result of enhanced metabolic stability conferred by the 5′-*E*- vinylphosphonate modification or better binding to hAgo2 compared to the 'natural' 5′-P.

Using the apo form of hAgo2 we were able to measure and compare binding affinities of several forms of guide RNAs to hAgo2. We showed that a guide with a 5′-*E*-VPu modification exhibits higher binding affinity to hAgo2 over both unmodified RNA and a 5′-P-containing RNA. This provides a rationale for the increased incorporation levels into hAgo2 and enhanced silencing of the 5′-*E*-VP modified RNAs.

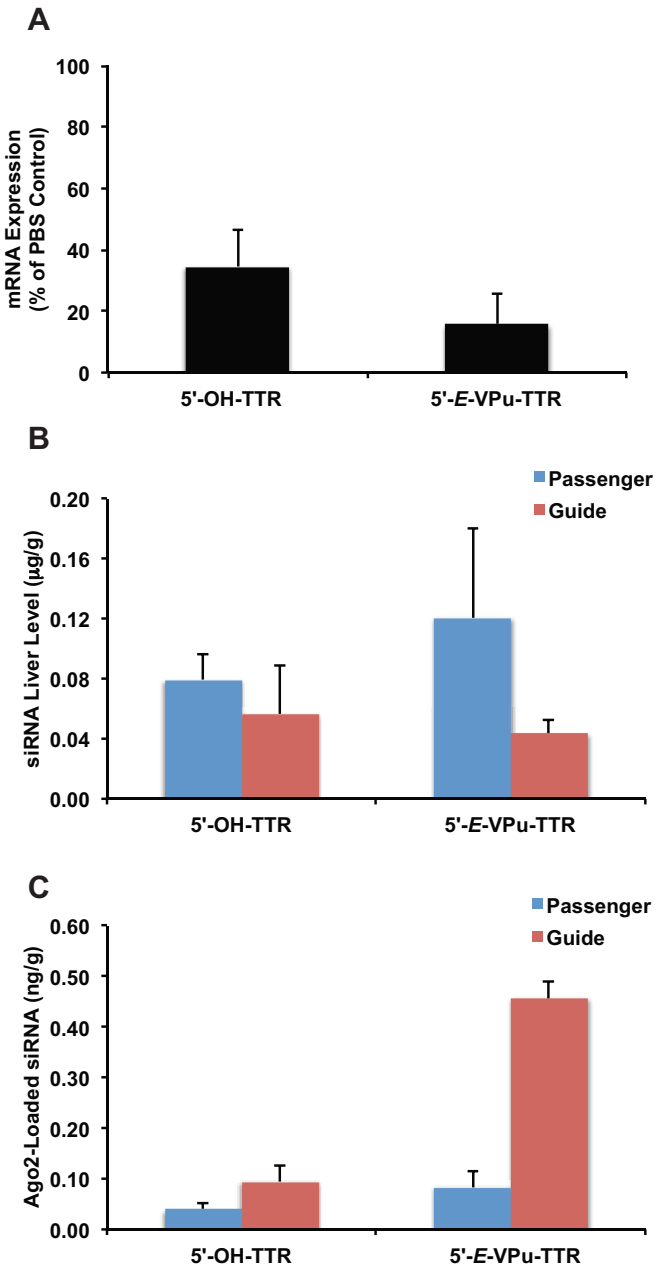

Figure 3. *In-vivo* quantification of mRNA and hAgo2 incorporated siRNA levels in the mouse liver. (**A**) levels of *TTR* mRNA in liver after treatment of mice with 5′-OH-TTR siRNA or 5′-*E*-VPu-TTR siRNA, $n = 3$. (**B**) Levels of guide (red) and passenger (blue) strands in livers of mice treated with 5′-OH-TTR siRNA or 5′-*E*-VPu-TTR siRNA, $n = 3$. (**C**) Levels of Ago2-incorporated guide (red) and passenger (blue) strands in livers of mice treated with 5′-OH-TTR siRNA or 5′-*E*-VPu-TTR siRNA, $n = 3$. Error bars present standard errors.

In addition, we determined the crystal structure of hAgo2 in complex with a guide RNA bearing a 5′-*E*-vinylphosphanate, 2′-OMe uridine modified nucleotide. Our crystal structure clearly shows how hAgo2 accommodates the modified nucleotide by adjusting the position of key residues that interact with the nucleotide while maintaining all the crucial interactions with the phosphate group. Indeed, previous studies have shown that despite

the fact that the 5′-binding pocket in the Mid domain of hAgo2 is heavily biased towards uracil, it can still bind all other bases and that higher affinity is mainly achieved by the presence of the phosphate group (1,37). For that reason we posit that modifications at the 5′-end position of the guide RNA are possible as long as the critical interactions with the phosphate moiety (or phosphate mimic) are kept intact as in the case of the 5′-*E*-VPu modification presented here.

While this manuscript was in preparation, a report, describing the structure of hAgo2 in complex with a chemically modified guide RNA carrying a similar 5′–*E*-VP modification on a thymidine nucleotide in addition to other RNA modifications, was published (32). Superposition of the two structures reveals some notable differences in the orientation of the modified guide RNA between the two structures (Supplementary Figure S2). First, the orientation of the 5′-E-VP thymidine in the 5′ binding pocket of hAgo2 is somewhat different than the one we see in the structure described here (Supplementary Figure S2A). While no change in the position of the 5′-E-VP is observed, the base and the ribose groups are shifted by 1 Å deeper into the 5′ binding pocket, a change that is accommodated by a movement of Y529 which is pushed backwards by 1 Å compared to our structure (Supplementary Figure S2B). The shift is likely due to the presence of the bulkier 2′-*O*-methoxyethyl (2′-*O*-MOE) modification compared to the 2'-OMe in our structure (38–40), which would otherwise clash with the side chain of Q548 (Supplementary Figure S2B). This shift in the ribose-base is accompanied by a repositioning of the phosphorothioate group between nucleotides 1 and 2 by 1 Å. There is also a lengthening of the H-bonds between the phosphorothioate and the N551 side chain and the amide backbone of Q548, compared with the normal phosphate, as one might expect from the different nature of these H-bonds. Finally, we observed a major change between the structures when comparing the positions of nucleotides 5 and 6 (the remaining residues were not resolved in the other study).

The guide strand in the two structures takes a different direction resulting in an increasing difference in position of 0.7–2.9 Å up to a 6 Å shift of the sugar and nucleobase of nucleotide 6 compared to the structure presented here. A similar difference was also noticed by the authors of that study when compared to an unmodified siRNA with the same sequence, suggesting that this difference is likely due to the additional modifications on the siRNA (Supplementary Figure S2A). Overall, comparing all three structures (unmodified, the 5′-*E*-VP-modified, and the extensively modified guide strands), it is clear that even minor modifications of 5′-phosphate result in nontrivial adjustments of the hAgo2 5′-P binding site.

In vivo siRNA loading of hAgo2 is driven by the use of short RNA duplexes (41,42), and requires the assistance of several other components such as Dicer, TRBP and the chaperon machinery (43–46), while hAgo2 loading *in vitro* requires a 5′-phosphorylated 20–23mer single-stranded RNA and the Argonaute protein (minimal RISC) without the need for any additional components (1). Our results indicate that 5′-*E*-VPu modified siRNAs can be efficiently loaded into hAgo2 and are superior to those carrying the natural 5′-P *in vitro* as well as *in vivo*. Moreover, the 5′-*E*-VPu modification that was used in GalNAc-conjugated siRNAs proved to be more efficient in silencing the endogenous levels of transthyretin (TTR) mRNA in mice compared to the same modified RNA with a 5′-OH instead of the 5′-*E*-VPu. Finally, we believe that since the hAgo2-guide RNA complex is extremely stable *in vitro* (23) and long lived *in vivo* (47,48), a combination of the increased metabolic stability of the modified RNAs, the inherent resilience of the hAgo-guide RNA complex and improved incorporation levels to hAgo2 could result in the enhanced and long lasting silencing effects of these molecules as therapeutic agents.

SUPPLEMENTARY DATA

Supplementary Data are available at NAR Online.

ACKNOWLEDGEMENTS

We are grateful to M.A. Maier, V. Jadhav, K. Charisse and R.G. Kallanthottathil for helpful discussions, A. Epstein for technical assistance with protein expression and purification, J. O'Shea for oligonucleotide synthesis and D. Foster for *in vitro* assays. We thank S. Ginell and B. Nocek for help at the Structural Biology Center at the Advanced Photon Source at Argonne National Laboratory, J. O'Shea for oligonucleotide synthesis and D. Foster for *in vitro* assays. Argonne is operated by UChicago Argonne, LLC, for the U.S. Department of Energy, Office of Biological and Environmental Research under contract DE-AC02-06CH11357.

FUNDING

Cold Spring Harbor Laboratory Women in Science Award (to L.J.); L.J. is an investigator of the Howard Hughes Medical Institute. Funding for open access charge: HHMI (to L.J.).

Conflict of interest statement. R.P., C.R.B., J.L.W., C.S.T. and M.M. are employees of Alnylam Pharmaceuticals.

REFERENCES

1. Rivas,F.V., Tolia,N.H., Song,J.-J., Aragon,J.P., Liu,J., Hannon,G.J. and Joshua-Tor,L. (2005) Purified Argonaute2 and an siRNA form recombinant human RISC. *Nat. Struct. Mol. Biol.*, **12**, 340–349.
2. Wee,L.M., Flores-Jasso,C.F., Salomon,W.E. and Zamore,P.D. (2012) Argonaute divides its RNA guide into domains with distinct functions and RNA-binding properties. *Cell*, **151**, 1055–1067.
3. Frank,F., Fabian,M.R., Stepinski,J., Jemielity,J., Darzynkiewicz,E., Sonenberg,N. and Nagar,B. (2011) Structural analysis of 5′-mRNA-cap interactions with the human AGO2 MID domain. *EMBO Rep.*, **12**, 415–420.
4. Boland,A., Tritschler,F., Heimstädt,S., Izaurralde,E. and Weichenrieder,O. (2010) Crystal structure and ligand binding of the MID domain of a eukaryotic Argonaute protein. *EMBO Rep.***11**, 522–527.
5. Boland,A., Huntzinger,E., Schmidt,S., Izaurralde,E. and Weichenrieder,O. (2011) Crystal structure of the MID-PIWI lobe of a eukaryotic Argonaute protein. *Proc. Natl. Acad. Sci. U.S.A.*, **108**, 10466–10471.
6. Sehgal,A., Barros,S., Ivanciu,L., Cooley,B., Qin,J., Racie,T., Hettinger,J., Carioto,M., Jiang,Y., Brodsky,J. *et al.* (2015) An RNAi therapeutic targeting antithrombin to rebalance the coagulation system and promote hemostasis in hemophilia. *Nat. Med.*, **21**, 492–497.

7. Chan,A., Liebow,A., Yasuda,M., Gan,L., Racie,T., Maier,M., Kuchimanchi,S., Foster,D., Milstein,S., Charisse,K. *et al.* (2015) Preclinical development of a subcutaneous ALAS1 RNAi therapeutic for treatment of hepatic porphyrias using circulating RNA quantification. *Mol. Ther. Nucleic Acids*, **4**, e263.
8. Nair,J.K., Willoughby,J.L.S., Chan,A., Charisse,K., Alam,M.R., Wang,Q., Hoekstra,M., Kandasamy,P., Kel'in,A.V., Milstein,S. *et al.* (2014) Multivalent N-acetylgalactosamine-conjugated siRNA localizes in hepatocytes and elicits robust RNAi-mediated gene silencing. *J. Am. Chem. Soc.*, **136**, 16958–16961.
9. Prakash,T.P., Lima,W.F., Murray,H.M., Elbashir,S., Cantley,W., Foster,D., Jayaraman,M., Chappell,A.E., Manoharan,M., Swayze,E.E. *et al.* (2013) Lipid nanoparticles improve activity of single-stranded siRNA and gapmer antisense oligonucleotides in animals. *ACS Chem. Biol.*, **8**, 1402–1406.
10. Parmar,R., Willoughby,J.L.S., Liu,J., Foster,D.J., Brigham,B., Theile,C.S., Charisse,K., Akinc,A., Guidry,E., Pei,Y. *et al.* (2016) 5′-(E)-Vinylphosphonate: a stable phosphate mimic can improve the RNAi activity of siRNA-GalNAc conjugates. *ChemBioChem*, **17**, 985–989.
11. Heydrick,S.J., Lardeux,B.R. and Mortimore,G.E. (1991) Uptake and degradation of cytoplasmic RNA by hepatic lysosomes. Quantitative relationship to RNA turnover. *J. Biol. Chem.*, **266**, 8790–8796.
12. Lima,W.F., Prakash,T.P., Murray,H.M., Kinberger,G.A., Li,W., Chappell,A.E., Li,C.S., Murray,S.F., Gaus,H., Seth,P.P. *et al.* (2012) Single-stranded siRNAs activate RNAi in animals. *Cell*, **150**, 883–894.
13. Yu,D., Pendergraff,H., Liu,J., Kordasiewicz,H.B., Cleveland,D.W., Swayze,E.E., Lima,W.F., Crooke,S.T., Prakash,T.P. and Corey,D.R. (2012) Single-stranded RNAs use RNAi to potently and allele-selectively inhibit mutant huntingtin expression. *Cell*, **150**, 895–908.
14. Hu,J., Liu,J., Narayanannair,K.J., Lackey,J.G., Kuchimanchi,S., Rajeev,K.G., Manoharan,M., Swayze,E.E., Lima,W.F., Prakash,T.P. *et al.* (2014) Allele-selective inhibition of mutant Atrophin-1 expression by duplex and single-stranded RNAs. *Biochemistry*, **53**, 4510–4518.
15. Prakash,T.P., Lima,W.F., Murray,H.M., Li,W., Kinberger,G.A., Chappell,A.E., Gaus,H., Seth,P.P., Bhat,B., Crooke,S.T. *et al.* (2015) Identification of metabolically stable 5′-phosphate analogs that support single-stranded siRNA activity. *Nucleic Acids Res.*, **43**, 2993–3011.
16. Hampton,A., Kappler,F. and Perini,F. (1976) Evidence for the conformation about the C(5′)-O(5′) bond of AMP complexed to AMP kinase: substrate properties of a vinyl phosphonate analog of AMP. *Bioorg. Chem.*, **5**, 31–35.
17. Harborth,J., Elbashir,S.M., Vandenburgh,K., Manninga,H., Scaringe,S.A., Weber,K. and Tuschl,T. (2003) Sequence, chemical, and structural variation of small interfering RNAs and short hairpin RNAs and the effect on mammalian gene silencing. *Antisense Nucleic Acid Drug Dev.*, **13**, 83–105.
18. Manoharan,M. (2004) RNA interference and chemically modified small interfering RNAs. *Curr. Opin. Chem. Biol.*, **8**, 570–579.
19. Allerson,C.R., Sioufi,N., Jarres,R., Prakash,T.P., Naik,N., Berdeja,A., Wanders,L., Griffey,R.H., Swayze,E.E. and Bhat,B. (2005) Fully 2'-modified oligonucleotide duplexes with improved in vitro potency and stability compared to unmodified small interfering RNA. *J. Med. Chem.*, **48**, 901–904.
20. Prakash,T.P., Allerson,C.R., Dande,P., Vickers,T.A., Sioufi,N., Jarres,R., Baker,B.F., Swayze,E.E., Griffey,R.H. and Bhat,B. (2005) Positional effect of chemical modifications on short interference RNA activity in mammalian cells. *J. Med. Chem.*, **48**, 4247–4253.
21. Bumcrot,D., Manoharan,M., Koteliansky,V. and Sah,D.W.Y. (2006) RNAi therapeutics: a potential new class of pharmaceutical drugs. *Nat. Chem. Biol.*, **2**, 711–719.
22. Watts,J.K., Deleavey,G.F. and Damha,M.J. (2008) Chemically modified siRNA: tools and applications. *Drug Discov. Today*, **13**, 842–855.
23. Elkayam,E., Kuhn,C.-D., Tocilj,A., Haase,A.D., Greene,E.M., Hannon,G.J. and Joshua-Tor,L. (2012) The structure of human argonaute-2 in complex with miR-20a. *Cell*, **150**, 100–110.
24. Vonrhein,C., Flensburg,C., Keller,P., Sharff,A., Smart,O., Paciorek,W., Womack,T. and Bricogne,G. (2011) Data processing and analysis with the autoPROC toolbox. *Acta Crystallogr. D Biol. Crystallogr.*, **67**, 293–302.
25. McCoy,A.J. (2007) Solving structures of protein complexes by molecular replacement with Phaser. *Acta Crystallogr. D Biol. Crystallogr.*, **63**, 32–41.
26. Adams,P.D., Afonine,P.V., Bunkóczi,G., Chen,V.B., Davis,I.W., Echols,N., Headd,J.J., Hung,L.-W., Kapral,G.J., Grosse-Kunstleve,R.W. *et al.* (2010) PHENIX: a comprehensive Python-based system for macromolecular structure solution. *Acta Crystallogr. D Biol. Crystallogr.*, **66**, 213–221.
27. Emsley,P., Lohkamp,B., Scott,W.G. and Cowtan,K. (2010) Features and development of Coot. *Acta Crystallogr. D Biol. Crystallogr.*, **66**, 486–501.
28. Faehnle,C.R., Elkayam,E., Haase,A.D., Hannon,G.J. and Joshua-Tor,L. (2013) The making of a slicer: activation of human Argonaute-1. *Cell Rep.*, **3**, 1901–1909.
29. Pei,Y., Hancock,P.J., Zhang,H., Bartz,R., Cherrin,C., Innocent,N., Pomerantz,C.J., Seitzer,J., Koser,M.L., Abrams,M.T. *et al.* (2010) Quantitative evaluation of siRNA delivery in vivo. *RNA*, **16**, 2553–2563.
30. Chen,C. (2005) Real-time quantification of microRNAs by stem-loop RT-PCR. *Nucleic Acids Research*, **33**, e179.
31. Saraiva,M.J., Costa,P.P., Birken,S. and Goodman,D.S. (1983) Presence of an abnormal transthyretin (prealbumin) in Portuguese patients with familial amyloidotic polyneuropathy. *Trans. Assoc. Am. Physicians*, **96**, 261–270.
32. Schirle,N.T., Kinberger,G.A., Murray,H.F., Lima,W.F., Prakash,T.P. and MacRae,I.J. (2016) Structural analysis of human Argonaute-2 bound to a modified siRNA guide. *J. Am. Chem. Soc.*, **138**, 8694–8697.
33. Schirle,N.T. and MacRae,I.J. (2012) The crystal structure of human Argonaute2. *Science*, **336**, 1037–1040.
34. Nakanishi,K., Ascano,M., Gogakos,T., Ishibe-Murakami,S., Serganov,A.A., Briskin,D., Morozov,P., Tuschl,T. and Patel,D.J. (2013) Eukaryote-specific insertion elements control human ARGONAUTE slicer activity. *Cell Rep.*, **3**, 1893–1900.
35. Schirle,N.T., Sheu-Gruttadauria,J. and MacRae,I.J. (2014) Structural basis for microRNA targeting. *Science*, **346**, 608–613.
36. Lima,W.F., Wu,H., Nichols,J.G., Sun,H., Murray,H.M. and Crooke,S.T. (2009) Binding and cleavage specificities of human Argonaute2. *J. Biol. Chem.*, **284**, 26017–26028.
37. Frank,F., Sonenberg,N. and Nagar,B. (2010) Structural basis for 5′-nucleotide base-specific recognition of guide RNA by human AGO2. *Nature*, **465**, 818–822.
38. Teplova,M., Minasov,G., Tereshko,V., Inamati,G.B., Cook,P.D., Manoharan,M. and Egli,M. (1999) Crystal structure and improved antisense properties of 2'-O-(2-methoxyethyl)-RNA. *Nat. Struct. Mol. Biol.*, **6**, 535–539.
39. Manoharan,M., Akinc,A., Pandey,R.K., Qin,J., Hadwiger,P., John,M., Mills,K., Charisse,K., Maier,M.A., Nechev,L. *et al.* (2011) Unique gene-silencing and structural properties of 2′-fluoro-modified siRNAs. *Angew. Chem. Int. Ed.*, **50**, 2284–2288.
40. Lubini,P., Zürcher,W. and Egli,M. (1994) Stabilizing effects of the RNA 2′-substituent: crystal structure of an oligodeoxynucleotide duplex containing 2′-O-methylated adenosines. *Chem. Biol.*, **1**, 39–45.
41. Fire,A., Xu,S., Montgomery,M.K., Kostas,S.A., Driver,S.E. and Mello,C.C. (1998) Potent and specific genetic interference by double-stranded RNA in Caenorhabditis elegans. *Nature*, **391**, 806–811.
42. Matranga,C., Tomari,Y., Shin,C., Bartel,D.P. and Zamore,P.D. (2005) Passenger-strand cleavage facilitates assembly of siRNA into Ago2-containing RNAi enzyme complexes. *Cell*, **123**, 607–620.
43. Liu,Q., Rand,T.A., Kalidas,S., Du,F., Kim,H.-E., Smith,D.P. and Wang,X. (2003) R2D2, a bridge between the initiation and effector steps of the Drosophila RNAi pathway. *Science*, **301**, 1921–1925.
44. Pham,J.W., Pellino,J.L., Lee,Y.S., Carthew,R.W. and Sontheimer,E.J. (2004) A Dicer-2-dependent 80S complex cleaves targeted mRNAs during RNAi in Drosophila. *Cell*, **117**, 83–94.
45. Iwasaki,S., Kobayashi,M., Yoda,M., Sakaguchi,Y., Katsuma,S., Suzuki,T. and Tomari,Y. (2010) Hsc70/Hsp90 chaperone machinery mediates ATP-dependent RISC loading of small RNA duplexes. *Molecular Cell*, **39**, 292–299.

46. Iwasaki,S., Sasaki,H.M., Sakaguchi,Y., Suzuki,T., Tadakuma,H. and Tomari,Y. (2015) Defining fundamental steps in the assembly of the Drosophila RNAi enzyme complex. *Nature*, **521**, 533–536.
47. Olejniczak,S.H., La Rocca,G., Gruber,J.J. and Thompson,C.B. (2013) Long-lived microRNA-Argonaute complexes in quiescent cells can be activated to regulate mitogenic responses. *Proc. Natl. Acad. Sci. U.S.A.*, **110**, 157–162.
48. Martinez,N.J. and Gregory,R.I. (2013) Argonaute2 expression is post-transcriptionally coupled to microRNA abundance. *RNA*, **19**, 605–612.